Acta of Bioengineering and Biomechanics
Vol. 24, No. 1, 2022

Original paper
DOI: 10.37190/ABB-01989-2021-02

Discrete phase model of blood flow in a roughness microchannel simulating the formation of pseudointima

MAGDALENA KOPERNIK[1]*, KARINA DYRDA, PRZEMYSŁAW KURTYKA[2, 3], ROMAN MAJOR[3]

[1] AGH University Science and Technology, Kraków, Poland.
[2] Foundation for Cardiac Surgery Development, Institute of Heart Prostheses, Zabrze, Poland.
[3] Institute of Metallurgy and Materials Science, Polish Academy of Sciences, Kraków, Poland.

Purpose: The goal of the present study was the development of discrete phase model to simulate the phenomenon of backfilling a morphologically complex surface by red blood cells (RBCs) in a flow microchannel and to anticipate the conditions of forming a pseudointima. The objective of the experimental studies that inspired the development of the simulation was to create a surface that stimulates the formation of the pseudointima layer. *Methods*: The finite volume method (FVM) and discrete particle method (DPM) were applied to develop the target model. In addition, a mixture model and a roughness model of bottom layer were tested in the present study to show their influence on simulation the phenomenon of backfilling a morphologically complex surface by RBCs in a flow microchannel. *Results*: Numerical models were developed including: a) FVM models to compare the effect of applying boundary conditions with/without roughness and cubes, as well as the analysis of their influence on blood velocity and shear stress; b) mixture models to compare the effect of applying different boundary conditions and cubes on computed results; c) DPM models to compare the effect of applying and not applying roughness as a boundary condition; d) DPM models with a morphologically complex surface and RBCs collisions to present RBCs concentration, velocity and time distributions during flow in a channel. *Conclusions*: The analysis carried out for the developed numerical models indicates that DPM model with cubes computes the best results. It also shows the backfilling of a morphologically complex surface of the bottom microchannel with RBCs.

Key words: *finite volume method (FVM), disperse particle method (DPM), mixture model, red blood cells (RBCs), blood models, microchannel, pseudointima*

1. Introduction

The analysis of the phenomena related to the blood flow in the microchannels is focused on macroscopic flow phenomena such as Fahraeus effect and Fahraeus–Lindqvist effect [49]. For microtubes diameters less than 300 μm, Fahraeus and Lindqvist observed that the apparent blood viscosity decreases as the microtube diameter becomes smaller. The experimental research tools used for these purposes are micro-PIV (particle image velocimetry) and confocal micro-PIV techniques [52].

Experimental and numerical work on the modeling of the flow in microchannels and ensuring good compliance with the experiment is used, inter alia, mixture theory [27], discrete particle method [53] and SST k-ω turbulence model [53], [21]. The analysis of the flow in microchannels may also concern issues related to blood-contacting devices, which cause hemolysis [53]. In this work, the turbulence model will be used due to the need to analyze the effects of induced surface roughness.

The selection of rheological models for blood flow modeling in this work takes into account the relationship between the shear stress and the shear rate, for

* Corresponding author: Magdalena Kopernik, AGH University Science and Technology, al. Mickiewicza 30, 30-059 Kraków, Poland. E-mail: kopernik@agh.edu.pl
Received: November 22nd, 2021
Accepted for publication: February 10th, 2022

which the differences are more visible for different roughnesses [44] when the rheological model with well-separated yield stress is used [31]. The yield stress of blood is typically very small, on the order of 1 mPa, and consequently difficult to measure, and can be easily missed.

Fluids can be classified as compressible or incompressible and depending on whether their viscosity does not change applying a shear stress (Newtonian) or the viscosity changes applying a shear stress (non-Newtonian). For example, the Newtonian blood models with well distinguished yield stress are Casson model, Herschel–Bulkley model and Bingham model [15]. However, the non-Newtonian character of blood rheology was recognized scientifically fairly early, more than 100 years ago. The review of literature presented in [14] and in the Authors' previous works [28], [29] shows that it is recommended to use non-Newtonian blood models, like power law [29] and Herschel–Bulkley [28] for small blood channels. Many papers state that blood cannot be considered as a single phase homogeneous viscous fluid, especially in the narrowing arteries [42]. Theory of interacting continua for mixtures which treats blood as a two fluid mixture containing plasma, treated as a viscous fluid, and RBCs, treated as a concentrated suspension with hematocrit and shear rate dependent viscosity, with special modeling for the drag and lift forces [27]. This model has shown to have reasonable agreement with experiments conducted in a sudden expansion microchannel flow. Thus, the blood flow in small channels in the present paper will be also represented by the two-phase models.

Particle-based models are applied to simulate RBCs membrane dynamics, margination effects and heterogeneities [3]. In the present paper, a discrete phase model (DPM) of backfilling a morphologically complex surface by RBCs is developed to investigate the behavior of the RBCs from a Lagrangian view and a discrete perspective. The blood behavior in Lagrangian view is examined on the basis of a particle tracking of a RBC of blood plasma flow, whereas blood plasma behavior is considered in Eulerian view based on the assumption of a finite volume element in the fluid flow path. In modeling of RBC, primary blood plasma interaction a two way approach is considered, in which RBC fluid flow and carrier blood plasma flow interact with each other simultaneously.

The adhesion of RBCs has been the center of interest for years [15]. *In vivo*, these clustering processes could play a significant role in thrombi formations and in the blood coagulation, while the RBCs aggregation is responsible for the shear thinning behavior of blood. RBCs are the main part responsible for blood viscosity.

Influence on RBCs aggregation have [15]:

- sedimentation rate,
- fibrinogen and C-reactive protein;
- polysaccharides, dextran and hydroxyethyl starch (HES);
- hydrodynamic radius that is inhibiting the aggregation below ca. 4 nm, while the above ca. 4 nm the RBC aggregation is induced;
- colloidal osmotic pressure of the macromolecules as the main reason for rouleaux formation (depletion theory);
- adsorption of macromolecules onto the RBC membranes and hence a potential adhesion between two cells as the origin of rouleaux formations (bridging theory);
- shape of contact zones and the buckling phenomenon;
- interparticle distance, which is low for depletion (close to zero) and high for bridging (in the range of the radius of gyration of the macromolecules);
- temperature (could change the balance between the fundamental mechanics of RBCs aggregation).

Models that take aggregation of red blood cells into account are, for example, thixotropic models [19], [22] or molecular dynamics models [3], [28], which are not considered in this paper.

Textured biomaterial surfaces in implantable left ventricular assist devices induce development of a non-thrombotic neointimal surface and allow elimination of anticoagulation therapy in device recipients [8], [38], [47], [51], [55]. Characterization of the hematopoietic cells formed within the neointimal surfaces of these devices may contribute to our understanding of this unique neointima. By implanting textured surfaces in contact with blood, a rapid clotting process occurs on the surface. While this may seem like a negative for blood contact surfaces, the concept is that while clots form quickly on these surfaces, they are densely adherent and do not appear to embolise into the bloodstream in a clinically relevant way. Over time, additional blood cell interaction occurs, similar to an immune response. A heterogeneous layer containing platelets, monocytes, macrophages, giant cells, lymphocytes and pluripotent hematopoietic cells is deposited on the surface. It is postulated that pluripotent hematopoietic cells differentiate into fibroblasts, myofibroblasts and in some cases endothelial cells. Fibroblast cells can then secrete extracellular matrix components such as collagen, which is routinely detected on textured surfaces after prolonged implantation.

The goal of the present study is the development of DPM (discrete phase model) to simulate the phenomenon of backfilling a morphologically complex surface by RBCs in a flow microchannel and, in this way, to anticipate the hemodynamic conditions of forming the pseudointima.

2. Materials and methods

The chapter describes the FVM, mixture and DPM models, taking the theoretical background and experimental research that constitute the basis for their development into account.

2.1. Physical models

The section introduces motivation and experimental basis for developing a microchannel blood flow model with a modified surface.

2.1.1. Physical model of microchannel

Microchannels allow for the simulation of various physiological conditions in blood vessels, while the system applied in this work was also used in [9]. The developed system of microchannels [9] allows for defined shear stresses in long-term culture, imaging of living cells and immunofluorescence for the analysis of the response to shear stress, mimicking of shear stress conditions in microcapillary, venous and arterial flows, displacement and adhesion of suspended cells in media, 3D cell culture (interstitial flow).

The basic geometry of the system was designed in accordance with the data included in the instruction manual of the experimental setup, based on the μ-Slide I Luer plate described in [9]. The developed model consists of a rectangular polymer plate with dimensions of 25.5 × 75.5 mm and a thickness of 1.6 mm. There are sleeves 3.5 mm high, 1 mm thick with an outer diameter of 7 mm on the top wall. A tunnel was cut inside the plate to allow the medium to flow. The inlet and outlet ducts take the shape of a cylinder with a diameter of 5 mm and a height of 4.2 mm. These rollers are mounted on a rounded cuboid 50 mm long, 5 mm wide and 0.8 mm high.

On the basis of the first model, a modified layout shape was also built. The modification concerned the bottom wall of the channel, which was subjected to corrugation. The unevenness of the surface was introduced by cutting 150 μm cubes in the lower layer with a distance of 200 μm between them.

2.1.2. Physical model of surface morphology

The morphology of bottom channel was reached by using commercially pure titanium powders sintered in vacuum on Ti6Al7Nb substrate. Titanium powders differed in size and morphology. Two types of grains were used – in the form of regular spheres and irregular crystals in three gradations, taking the diameters of microspheres and the size of angular crystals into account. The regular and irregular patterns of bottom layer of channel had target roughness from R_a = 20 to 50 μm. The distance between deposited particles was in the range of 10–200 μm.

2.2. Numerical models

The method of describing numerical models included in this paper meets the criteria for numerical models placed in [13]. Simulations shown in this paper were run using Ansys Fluent 2021 R1 an Ansys Fluent R2 software due to the fact that the new version was launched during developing simulations. These two versions do not have meaningful differences and they do not have influence on computed results presented in this paper.

2.2.1. FVM and mixture models with roughness and cubes

The section presents detailed solutions for FVM and mixture models, which describe the turbulence model and roughness model, as well as the assumed values of parameters.

2.2.1.1. Theoretical background of roughness and mixture models

The k-ω SST turbulent model is focused on the precision of the k-ω model in the areas close to the wall. The k-ω SST model's transport equations which are used in the Ansys Fluent code are [26]:

$$\frac{\partial(\rho k)}{\partial t}+\frac{\partial}{\partial x_i}(\rho k u_i)=\frac{\partial}{\partial x_j}\left[L_k\frac{\partial k}{\partial x_j}\right]+A_k-B_k \quad (1)$$

$$\frac{\partial(\rho \omega)}{\partial t}+\frac{\partial}{\partial x_i}(\rho \omega u_i)=\frac{\partial}{\partial x_j}\left[L_\omega\frac{\partial \omega}{\partial x_j}\right]+A_\omega-B_\omega+C_\omega, \quad (2)$$

where: u_i – mean velocity, A_k – the production terms of k, B_k – production terms of k, A_ω – the production

terms of ω, B_k – dissipation terms of k, B_ω – dissipation terms of ω, L_k – the effective diffusivity of k, L_ω – the effective diffusivity of ω, and C_ω – the diffusion term.

For modeling surface roughness, the rough wall model is introduced in the Ansys Fluent which was adapted from [50]. To implement surface roughness in the Ansys Fluent, the roughness height (H_r) and the roughness constant (C) should be defined. The effects of surface roughness can be properly accounted for in CFD codes by modified wall law as follows [43]:

$$\frac{U_q u^1}{\tau_\omega / \rho} = \frac{1}{k_1} \ln\left[9.793 \frac{u^1 y_q}{\mu} \right], \tag{3}$$

where: U_q – velocity at the wall near the cell at centre point q, y_q – height at the centre point q of the cells near the wall, μ – viscosity, ΔG – roughness function, τ_ω – wall shear stress, k_1 – Karman constant, and u^*: the wall friction velocity which can be defined as [39]:

$$u^* = 0.55 k_q^{0.5}, \tag{4}$$

where k_q is the turbulent kinetic energy near the wall at point q of the cell. According to [10], ΔG for fully rough regime can be defined as:

$$\Delta G = \frac{1}{\kappa} \ln(1 + C H_S^+) \tag{5}$$

where: H_S^+ – nondimentional roughness height, and C – roughness constant.

The range of roughness constant is 0–1 and according to [26], who worked on impacts of roughness on the numerical centrifugal pumps using Ansys Fluent. However, in this work, the value of C is taken as 0.5. Moreover, the nondimensional roughness height is defined as:

$$H_S^+ = \frac{\rho u^* H_r}{\mu}. \tag{6}$$

In the Ansys Fluent, the whole roughness regime is subdivided into the three regimes, and the formulas proposed by Cebeci and Bradshaw based on Nikuradse's data [10] are adopted to compute ΔG for each regime.

For the transitional regime ($2.25 < H_S^+ \leq 90$) adopted in this paper:

$$\Delta G = \frac{1}{\kappa} \ln\left[\frac{H_S^+ - 2.25}{87.75} + C H_S^+ \right] \sin\{0.4258(\ln H_S^+ - 0.811)\}. \tag{7}$$

It is not physically meaningful to have a mesh size such that the wall-adjacent cell is smaller than the roughness height.

Eulerian multi-phase models can account for dispersed-continuous phase interactions and continuous-continuous phase interactions. Dispersed phases can be particles (solids), droplets (liquids) or bubbles (gas). They are dissolved in the continuous fluid. Dispersed phases typically have micrometer to millimeter in diameter. Continuous-continuous phase interactions form a discrete interface. They are immiscible with each other. Mixture models are a simplified version of the full Eulerian model for dispersed-continuous phase interactions. Volume-of-fluid (VOF) models are a simplified version of full Eulerian model for continuous-continuous phase interactions. Thus, the mixture model was selected in simulation of a blood flow in the present paper.

Eulerian model equations can be characterized by:

- a continuity/mass conservation equation is solved for each phase,
- the equation is multiplied by the volume fraction of the phase (r_q)

$$\frac{\partial (r_q \rho_q)}{\partial t} + \nabla \cdot (r_q \rho_q U_q) = \Sigma_{p=1}^N (m_{pq}^\bullet - m_{qp}^\bullet) \tag{8}$$

- we can get mass transfer between phases ($m_{pq}^\bullet$) during phase change processes (evaporation and condensation),
- $m_{pq}^\bullet \equiv m_{p \to q}^\bullet$ (from p to q).

Dispersed-continuous phase interactions can take any value of volume-fraction between 0 and 1. While, continuous-continuous phase interactions are restricted to a volume fraction of either 0 or 1 (except in the interface region).

A volume-fraction equation can be characterized by:

- A transport equation is solved for the volume-fraction for each additional phase.
- N-1 volume fraction equations are solved:

$$\frac{\partial r_q}{\partial t} + \nabla \cdot (r_q U_q) = 0 \tag{9}$$

- We can deduce the volume fraction of the primary phase, as the sum of volume-fractions must be equal to 1.

$$\Sigma_{q=1}^N r_q = 1. \tag{10}$$

- This approach is common to Eulerian, mixture and VOF models.

Interface capturing is adopted by the VOF and Eulerian models (if desired), and therefore will not be discussed in this section.

Eulerian model equations can be described as:

- A separate momentum and energy equation are solved for each phase.
- The phases share a common pressure filed (so p has no sub-script).

$$\frac{\partial(r_q\rho_q U_q)}{\partial t}+\nabla\cdot(r_q\rho_q U_q U_q) = -r_q\nabla p+\nabla\cdot\tau_q+\Sigma_{p=1}^{N}(D_{pq}+m_{pq}^{\bullet}U_{pq}-m_{qp}^{\bullet}U_{qp}). \quad (11)$$

- We get additional momentum transfer between phase p and phase q.
- Momentum is transferred by mass ($m_{pq}^{\bullet}$) and by other forces (D_{pq}).

Interphase drag/momentum transfer can be briefly discussed as follows:

- As a separate momentum equation is solved for each phase, we get a separate velocity filed for each phase at the cell centroid.
- The velocities are different due to a drag and other inter-phase forces.
- The inter-phase momentum transfer from $p \rightarrow q$ to is denoted D_{pq}.

Interphase drag can be described as follows:

- The primary phase moves at velocity U_q.
- The secondary phase moves at velocity U_p.

The drag force acting on the primary phase is (remember $\frac{1}{2}\rho U^2 A C_D$):

$$D_{pq}=\frac{1}{2}\rho_q C_D A(U_p-U_q)\,|U_p-U_q|. \quad (12)$$

- The drag force per unit volume (V):

$$D_{pq}=\frac{1}{2}\rho_q C_D \frac{A_P}{V}(U_p-U_q)\,|U_p-U_q|, \quad (13)$$

where: C_D – drag coefficient, $\frac{A_P}{V}$ – interfacial area per unit volume, ρ – density.

Interphase drag for dispersed-continuous phase interactions can be described using the most popular drag model, which is the Schiller–Naumann drag model:

$$C_D=\begin{cases}\frac{24}{Re}(1+0.15Re^{0.687}) & Re<1000\\ 0.44 & Re>1000\end{cases}, \quad (14)$$

$$Re=\frac{\rho_q\,|U_p-U_q|\,d_p}{\mu_q}. \quad (15)$$

The interfacial area per unit cell volume for dispersed spheres $\left(\frac{A_P}{V}\right)$ is:

$$\frac{A_P}{V}=\frac{Volume\ of\ spheres}{Volume\ of\ cell}*\frac{Surface\ area\ of\ spheres}{Volume\ of\ spheres}, \quad (16)$$

$$\frac{A_P}{V}=r_p\left(\frac{\pi d_p^2}{\pi d_p^3/6}\right), \quad (17)$$

$$\frac{A_P}{V}=\frac{6r_p}{d_p}. \quad (18)$$

If the spheres have different sizes, an additional transport equation for the interfacial area per unit volume is solved.

Summarizing, Eulerian multi-phase models solve mass, momentum and energy equations for each phase individually. Inter-phase momentum and heat transfer dictates how the phases interact with each other. Interphase drag is predominant momentum transfer mechanism.

2.2.1.2. FVM and mixture model assumptions

FVM (finite volume method) models and mixture models were developed in Ansys Fluent 2021 R1 software to compare the effect of applying different boundary conditions with, without roughness and cubes, as well as to investigate their influence on blood velocity and shear stress.

The simulations were run on a standard PC (Processor Intel® Core™ i7-10700 CPU, 2.9 GHz, 16 GB RAM). The simulations lasted for 1.87 s (1500 iterations) with time step of 0.00125 s. The FVM (finite volume method) mesh of a flow channel is composed of 488 078 cells and 954 329 nodes. The average element size is 0.18 mm. The cubes generated in bottom layer of FVM model of flow channel had dimensions of 150 μm and distance among them was 200 μm. The mesh quality parameters (element quality – 0.56, aspect ratio – 9.64, skewness – 0.19, orthogonal quality – 0.81) were very good and there were 6 layers of prism elements near walls of the FVM model. The side view of FVM mesh of flow channel with indicated bottom layer and cubes are shown in Fig. 1. The FVM model uses non-Newtonian blood power law [29] and the following coefficients of blood are assumed: density 1059 kg/m^3 [12], specific heat 3617 J/kgK [25], thermal conductivity 0.52 W/mK [52]. The inlet velocity of blood (FVM) and plasma (mixture model) is set to 0.04 m/s [9].

The pressure-based solver and absolute velocity formulation were selected for computational purpose. The pressure-velocity coupling scheme of solution was selected for computation with spatial discretization using gradient (least squares cell based) and tran-

sient formulation. The SST k-ω turbulence model [21], [53] was applied in all simulations.

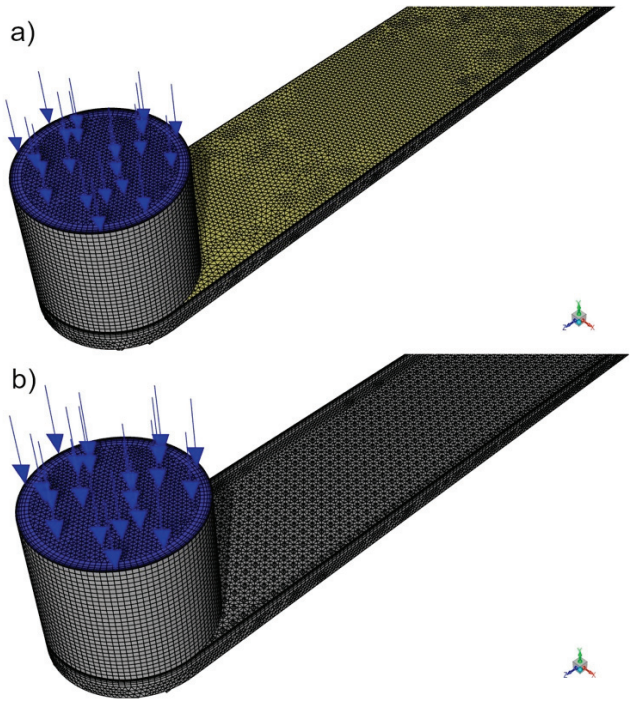

Fig. 1. Side view of FVM mesh of flow channel with indicated: a) inlet and bottom layer, and b) cubes

The bottom wall of the FVM and mixture models has a sand-grain roughness described by a standard roughness model with parameters: roughness height 25 μm and 40 μm, and roughness constant 0.5. The roughness model applied in the present paper has parameters of roughness based on experimental observation (see Section 2.1.2.) and they are correlated with element size according to the roughness model assumptions shown in the present paper.

Table 1. Parameters used in the two-phase blood model with references

parameters	red blood cells	blood plasma
density [kg/m^3]	1 090 [48]	1 040 [48]
specific heat [J/g°C]	0.87 [45]	3.93 [4]
thermal conductivity [W/mK]	2.36 [48]	9.93 [48]
viscosity [kg/ms]	0.0075 [24]	0.0015 [23]
molecular weight [kg/kmol]	0.0004 [18]	0.018 [1]

In Ansys Fluent, three different Euler–Euler multiphase models are available. In the present study the mixture one has been selected to model the two phases of blood: plasma and RBCs. As in the Eulerian model, the phases are treated as interpenetrating continua. The mixture model [5] can simulate phases by solving the momentum, continuity, and energy equations for the mixture, the volume fraction equations for the secondary phases, and algebraic expressions for the relative velocities. Parameters applied in computations for two-phase blood model are presented in Table 1 [1], [4], [18], [23], [24], [45], [48]. The mixture model uses Schiller–Naumann drag coefficient (compare Section 2.2.1.1).

2.2.2. DPM models with roughness and cubes

The section presents detailed solutions for DPM model, which describe the collisions model and Lagrangian Particle Tracking, as well as the assumed values of parameters.

2.2.2.1. Theoretical background of DPM model

Development of numerical model of collisions was preceded by experimental analysis of particle-wall collision process in a channel flow using particle tracking velocimetry [49]. The effect of wall on the collision process was analysed. Special attention was paid to the influence of wall roughness. For example it was found that wall roughness considerably alters the rebound behaviour of the particles and causes a re-dispersion of the particles. The experimental data were applied to develop an update of a wall collision model [30].

Numerical models of particle-fluid flows can be categorized into three methods, according to the treatment of the particulate and the fluid phases [54]: Eulerian-Eulerian methods, Lagrangian-Lagrangian methods and Eulerian-Lagrangian methods. In Eulerian-Eulerian methods, both the fluid and particulate phases are defined as interpenetrating continuous phases. A discrete phase model is used in the Lagrangian frame of reference to track particles' motion whereas the Eulerian formulation is simultaneously used for the continuous phase. Different forces (viscous drag, lift force, buoyancy etc.) acting on the Lagrangian particles along their trajectories are taken into account as well as a stochastic behavior of the surrounding turbulent flow.

In the Ansys Fluent software the particles are modelled as spheres with density and a particle size distribution based on the experimental distributions. The discrete phase is modelled using the Lagrangian approach with Fluent's DPM. The Lagrangian tracking method (compare Section 2.2.2.2.) is used to solve the individual trajectories of the theoretical particles by equating their inertia with external forces.

Two-way coupling, the exchange of momentum between the particles and fluid, is accounted for. The

physics includes: particle–wall collisions, particle–particle collisions and structure dependent drag. The spherical drag model of Morsi and Alexander [39] is used to model the particles. The effects of particle clustering and channel diameter on the drag of an isolated particle is modelled using a pressure balance model.

Particle-particle collisions are modelled using the Nanbu–Babovsky collision model [35]. This is a stochastic collision model where the probability of a collision between particles is based on the volume of particles within a cell and their relative velocities, as follows:

$$Pr_{col} = \Sigma_{j=1}^{N_j} \left\{ \frac{\pi}{4} (d_{p,i} + d_{p,j}) \, | u_{p,j} - u_{p,i} | \, n_{p,j} \right\} \Delta t_{col} \,, \tag{19}$$

where: d – diameter, u – velocity, p – discrete phase, i – index i, j – index j, Pr_{col} – collision probability, N – number of particles.

The collision partner is determined at random from the other particles in the cell as:

$$j = \lfloor \Phi N \rfloor + 1 \,, \tag{20}$$

where $\lfloor ... \rfloor$ is the integer part of the argument and Φ is a random number between [0, 1]. The model requires a limit on the collision time step,

$$\Delta t_{col,\max} = \frac{2}{\max(v_{ij} N_p)} \,, \tag{21}$$

where: this limiting collision timestep is less than the particle time step, the collision loop is repeated until the sum of the collision time steps is greater. Thus, the model resolves the expected number of collisions. The post collision velocities are calculated from the impulse equations.

The general form of collision model algorithm [20] compromises the following items:

- Call to the collision routine by the Lagrangian solver supplying the necessary variables.
- Calculation of the instantaneous velocity of the virtual collision partner.
- Determination of the collision probability and decision whether or not a collision occurs.
  - If a collision takes place
- the position of the virtual collision partner is determined and
- the binary collision is calculated deterministically;
  - if there is no collision the velocities remain unchanged.
- The fictitious particle is discarded.
- The trajectory calculation of the current real particle is continued until it is completed.
- For all trajectories the averaging procedure is carried out to obtain local statistical moments in each control volume.

2.2.2.2. DPM models assumptions

DPM models were developed to compare the effect of applying and not applying roughness as a boundary condition, and finally the DPM models with cubes were implemented to present distributions of RBCs concentration, velocity and RBCs residence time in the flow channel.

A DPM model of backfilling a morphologically complex surface by RBCs is developed to investigate the behavior of the RBCs from a Lagrangian view and a discrete perspective. The blood behavior in Lagrangian view is examined on the basis of a particle tracking of a RBC of blood plasma flow; Whereas blood plasma behavior is considered in Eulerian view based on the assumption of a finite volume element in the fluid flow path. In modeling of RBC – primary blood plasma interaction a two-way approach is considered, in which RBC fluid flow and carrier blood plasma flow interact with each other simultaneously.

Lagrangian Particle Tracking (LPT) [36] in Ansys Fluent 2021 R2 software is applied to show the effect of backfilling the regularly morphologically complex surface of sample by RBCs. The numerical procedure for carrying out Lagrangian Particle Tracking for red blood cells in the Ansys Fluent is as following:

– calculation of Reynolds number using RBC velocity from the previous time step / initial velocity,
– calculation of drag coefficient from Reynolds number using the Schiller–Neumann drag model,
– solution of the force balance to calculate new RBC velocity,
– update of the RBC position using the new velocity and time step,
– repetition of the procedure until the RBC times out / terminates.

The DPM simulations were run using computing unit DELL T7910 equipped with two processors (Intel® Xeon®CPU E5-2620 v3 @ 2.40GHz) in total of 12 cores, 128 GB DDR4 RAM and NVIDIA Quadro K5200 graphics card (8 GB GDDR5 (Hynix)).

The FVM meshes, turbulence model, inlet velocity and boundary conditions are the same as for models introduced in Section 2.2.1.2.

The diameter of RBCs is assumed from 5 μm to 10 μm using statistical diameter distribution and the average diameter is 7.5 μm [11].

The value of relaxation time informs how the particles respond to changes in the flow [36]. Red blood cell relaxation time is equal:

$$t_{RBC} = \frac{\rho_{RBC} d_{RBC}^2}{18\mu}, \tag{22}$$

where: ρ_{RBC} – red blood cell density, d_{RBC} – average diameter of red blood cells, μ – viscosity of blood plasma. The value of *RBC* maximal relaxation time is 4.037 μs.

The rotation of RBCs is enabled. The density of plasma is 1040 kg/m^3, specific heat is 3930 J/kgK, thermal conductivity is 9.93 W/mK and viscosity is 0.0015 kg/ms [4], [48]. The density of RBCs is equal to 1090 kg/m^3 and specific heat is equal to 870 J/kgK [45], [48]. Viscosity of red blood cells is set to 0.0075 kg/ms and their surface tension is set to $5 \cdot 10^{-6}$ N/m [2], [24].

The particles and plasma are injected in normal direction to the inlet. The total flow rate of *RBC*s is $1 \cdot 10^{-10}$ kg/s, *RBC*s time step is equal to $1.0 \cdot 10^{-5}$ and the maximum number of iterations of DPM model is set to 100 000. The plasma velocity is set to 0.04 m/s [9]. The boundary condition of *RBC*s phase is assumed as escape, however *RBC*s can be reflected from the ground. The friction coefficient is set to 0.2 [17].

3. Results

The computed results shown in this section are independent on size of time step, number of iterations and density or quality of computational mesh. The results are considered as distributions of velocity, shear stress for FVM, mixture and DPM models, as well as distributions of particle residence time, concentration and diameter for DPM models. The results are analysed in selected cross-sections of flow channel and presented in Fig. 2 (bottom plane of flow channel and cross-sections 1–3: beginning, middle and end of the flow channel).

The aim of the analysis of the results is to compare the influence of the boundary condition (roughness, cubes) on the flow parameters (velocity, shear stress) in all models, as well as determining the influence of the boundary condition (roughness, cubes) on the parameters important for the backfilling process (particle residence time, concentration) in the DPM models.

The computed flow parameters (velocity and wall shear stress) for FVM, mixture and DPM models are

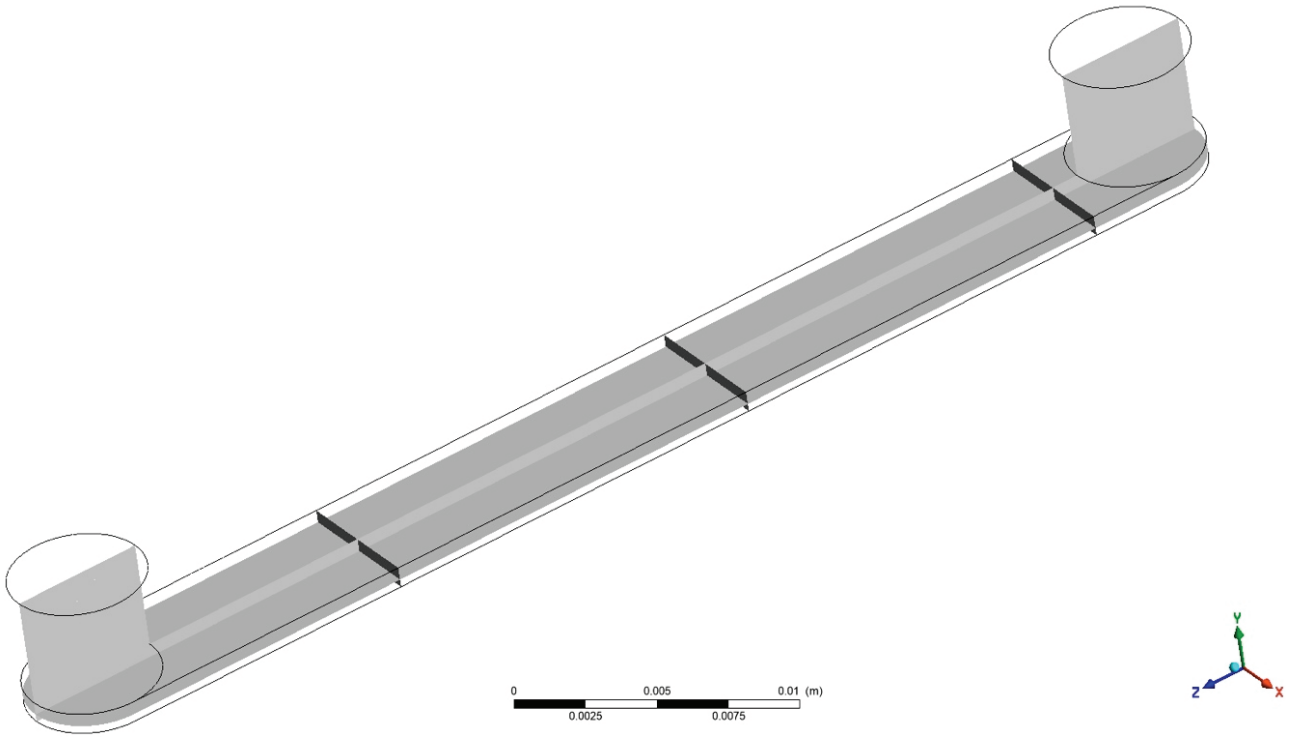

Fig. 2. Planes of model of flow channel considered in analysis

shown in Figs. 3–5. The backfilling process parameters (*RBC*s concentration, residence time) and flow parameters (velocity and wall shear stress) for DPM models are presented in Figs. 6–8.

(a)

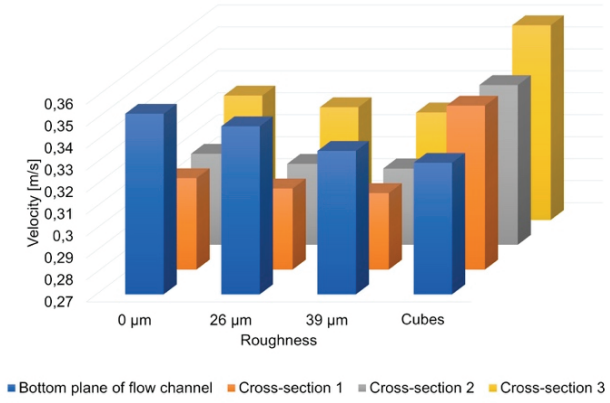

(b)

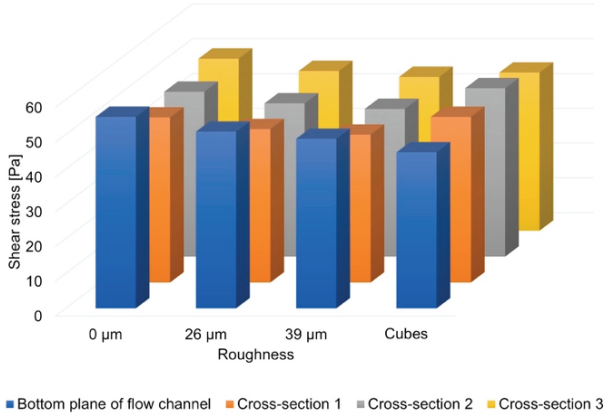

Fig. 3. Flow results of FVM model: (a) velocity, (b) wall shear stress for different boundary conditions

4. Discussion

In the single-phase model, applying roughness decreases the flow velocity along the bottom wall of the channel (Fig. 3a). The greatest reduction in flow velocity is visible for the model with cubes along the bottom wall of the channel and the highest velocity values in the flow channel are computed for the model with cubes.

In the single-phase model, the application of roughness slightly reduces the shear stresses along the bottom wall of the flow channel (Fig. 3b), however, the reduction of stresses is the greatest for the model with cubes. In all single-phase models and in all analyzed cross-sections of the channel, the shear stresses remain almost constant (several dozen pascals), the highest shear stress values are computed in the flow channel for the model without roughness. The values of shear stresses obtained in the flow channel with the use of single-phase models are comparable to the values presented in the literature, e.g., for flows through similar microfluidic systems and through small vessels with stenosis and (a dozen to over a hundred Pascals) [32], [34].

From the point of view of blood contact devices, it is therefore important to better understand the relationship between shear stress, exposure time and blood damage. An example of blood damage is not only hemolysis or activation of platelets, but also thrombosis and embolism as well as the destruction of von Willebrand factor (vWf). According to the literature, hemolysis occurs at shear stress level (SSL) >150 Pa, activation of thrombocytes >50 Pa and degradation of von Willebrand factor >9 Pa [16].

In the mixture model (Fig. 4a), the use of roughness does not affect the flow velocity in the channel, the analyzed models show a similar level of flow velocity, the differences in values of flow parameters among different parts of the flow channel are also poorly visible. The use of cubes in the mixture model increases the flow velocity along the bottom wall of the flow channel compared to the other mixture models. In all mixture models, except for the mixture model with cubes, the flow velocity along the bottom wall of the channel is significantly lower than in the other models (single-phase and DPM).

For the mixture model (Figure 4b), the shear stresses remain at the level of a few Pa and are by an order of magnitude lower than the shear stresses computed for the single-phase model. In the mixture model, the shear stress level is the lowest on the bottom channel wall for the model without roughness, while the highest values are for the model with cubes on the bottom channel wall and in the middle of the flow channel. In mixture models with roughness, the level of shear stresses is the same for a particular model in different sections of the flow channel. Two-phase models show lower values of computed shear stresses [29] than single-phase models, which also has occurred in the present paper. Two-phase models are less prone to disturbance, which is visible in small differences between the calculated values of shear stresses and flow velocity for different parts of the channel for two-phase models with different boundary conditions, except for the model with cubes. For example, low shear stress values comparable to computed for two-phase models in the present paper were obtained in the experiment presented in [7] for micro-

channels with blood and in multi-phase blood models applied for stenosed arteries in [6].

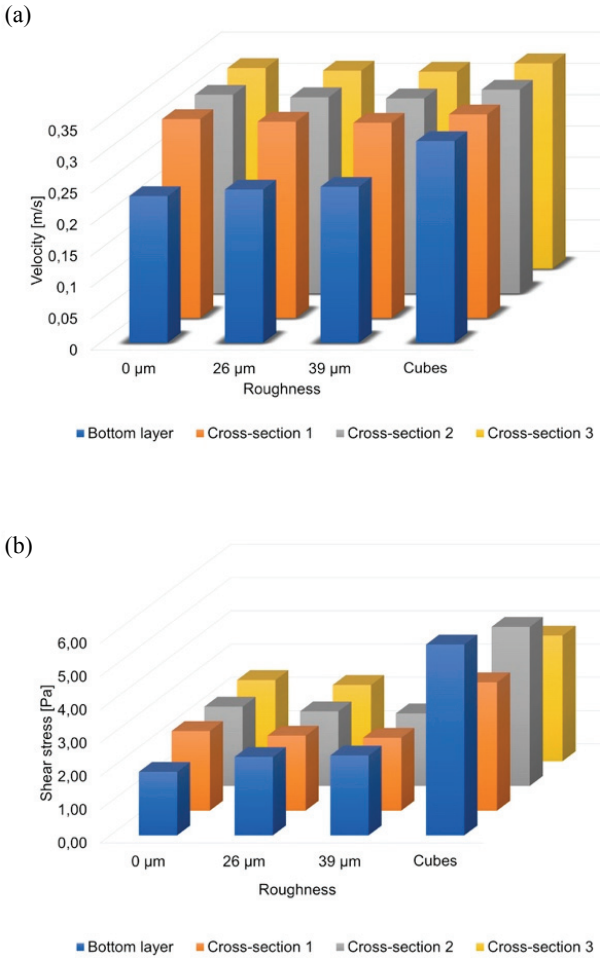

Fig. 4. Flow results of mixture model: (a) velocity, (b) wall shear stress for different boundary conditions

Velocity analysis for DPM models (Fig. 5a) shows that the differences in velocity values are significant for the DPM models compared to the single-phase and mixture models. The highest flow velocities are observed for the DPM model without roughness, while the lowest values, similar to the values for single-phase and mixture models, occur for the DPM model with cubes.

For DPM models (Fig. 5b), the lowest values of shear stresses occur at the bottom of the channel and then increase but remain constant for the particular model. The lowest shear stresses occur for the model with cubes and are comparable to the shear stress level of the mixture model (a few Pa). Roughness causes a decrease in shear stresses in the DPM models, the higher the roughness, the lower the shear stress. In the DPM models in literature, the values of shear stresses for microfluidic systems may reach several hundred pascals [53], and for vessels with stenoses they are about a dozen or so pascals [46]. Thus, the values obtained in this paper for shear stresses in the DPM model are comparable to the results obtained by other authors for similar flow systems.

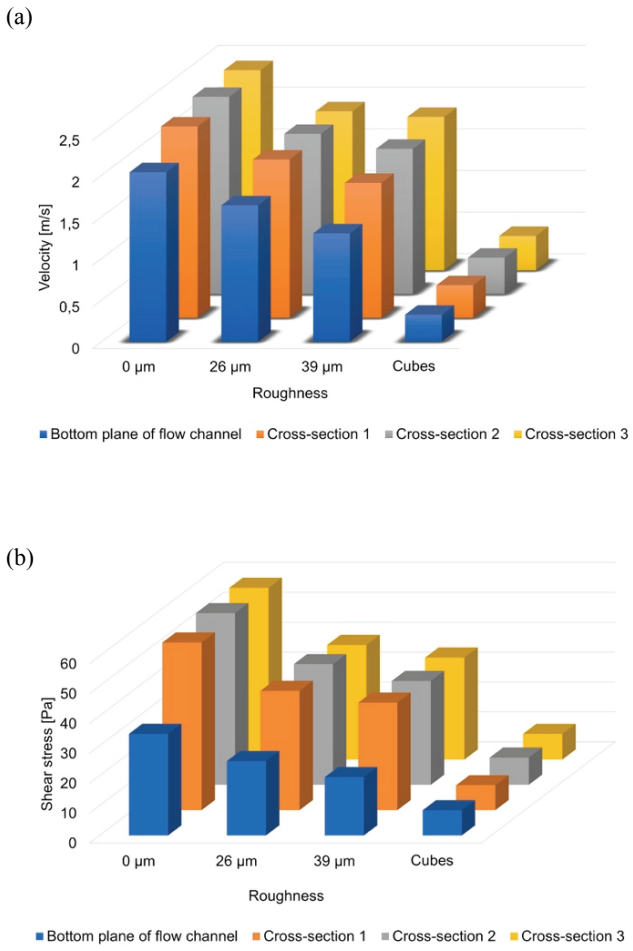

Fig. 5. Flow results of DPM model: (a) velocity, (b) wall shear stress for different boundary conditions

A comparative analysis of single-phase, mixture models and particle models shows that the influence of particles on the flow parameters is significant and the selection of the model with particles is appropriate in the context of micro-level phenomena, which one or two-phase models cannot capture.

The increase in roughness (Fig. 6) results in an increase in red blood cell concentration, while the greatest increase is observed for the DPM model with cubes.

In the DPM models, red blood cells are represented by spheres that lose their ability to deform and they tend to increase the viscosity [33]. However, at concentrations bigger than 50%, the displacement decreases. At HCT >50%, although the crowded environment leads to an increase of the cell deformation, it

also limits the magnitude of the *RBC* radial dispersion. However, in a healthy human body, HCT typically ranges between 40.7–50.3% for men and 36.1–44.3% for women. In the suspension of spheres, at 50% concentration, the viscosity increases exponentially making them difficult to flow. Due to the fact that blood density above 50% *RBC* does not occur in natural conditions for healthy patients, such a case was not considered.

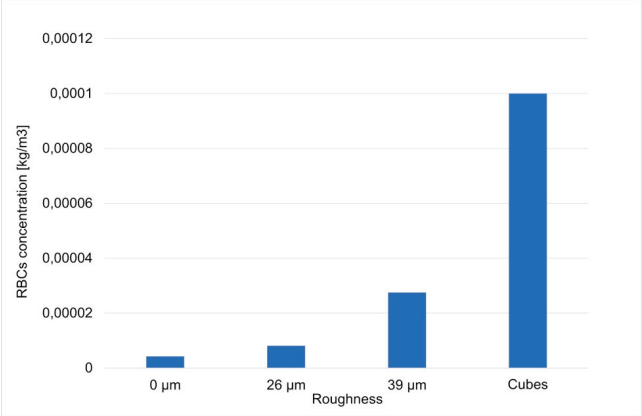

Fig. 6. RBCs concentration for different boundary conditions

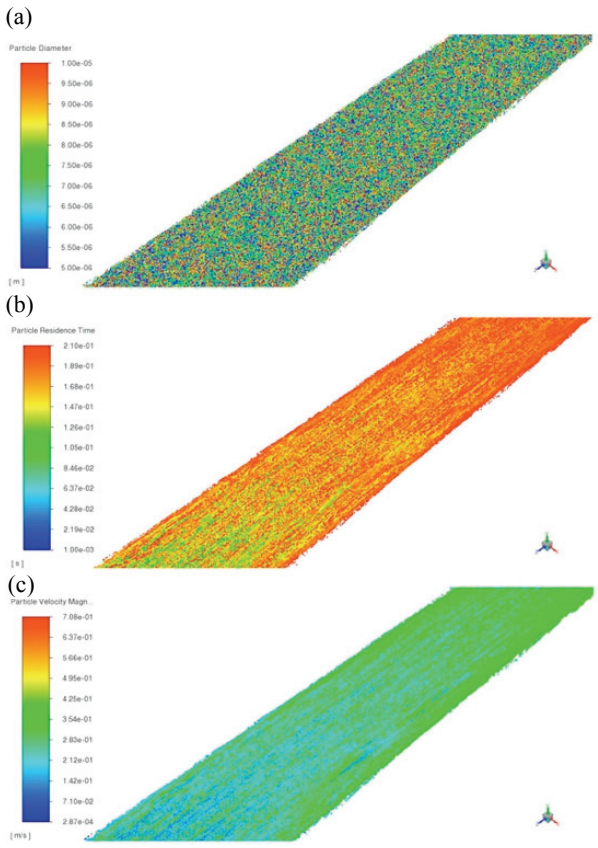

Fig. 7. Results of DPM model of backfilling a morphologically complex surface by *RBC*s: (a) distribution of *RBC*s diameter, (b) distribution of *RBC*s residence time, (c) distribution of *RBC*s velocity

In the developed DPM model, the hematocrit is high, the concentration of blood cells is high, so the viscosity also increases. This also has to do with the reduction of shear stress (increased viscosity) and the formation of rolls [40].

Spheres have axial migration, however the spheres not always migrate toward the centre. The spheres near the wall move towards the centre whereas the ones in the centre move towards the wall. At the end they reach an equilibrium position. This effect is known as tubular pinch effect [33].

The selected results of DPM model of backfilling a morphologically complex surface by *RBC*s are shown in Fig. 7 as distributions of *RBC*s diameter, residence

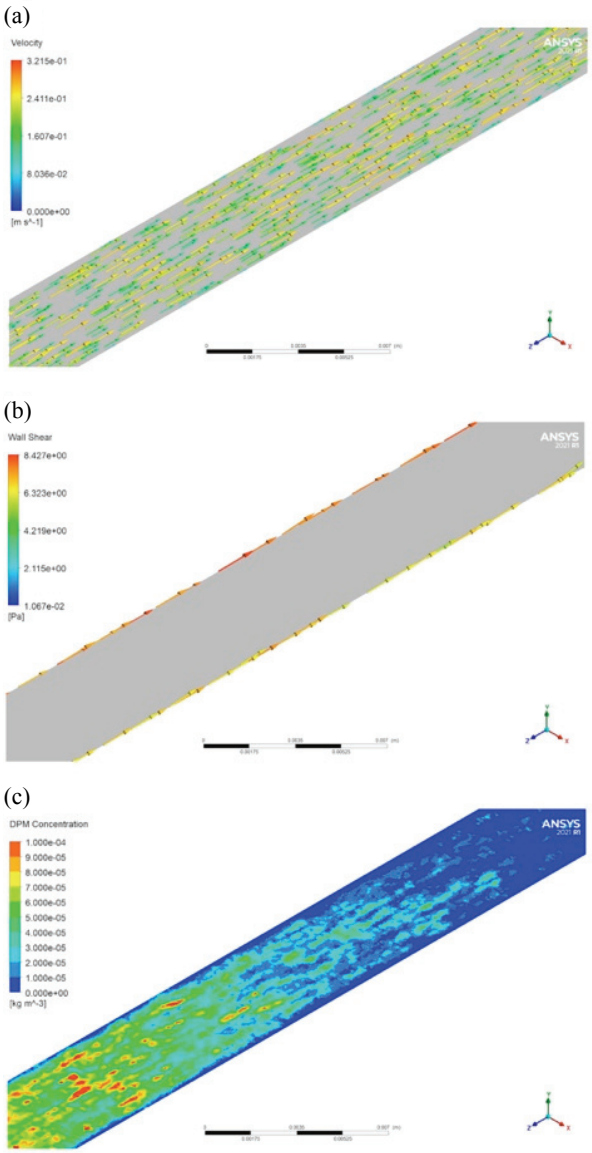

Fig. 8. Results of DPM model of backfilling a morphologically complex surface by *RBC*s in selected cross-sections: (a) vector distribution of velocity in the bottom plane, (b) vector distribution of shear stress in the bottom plane, (c) distribution of *RBC*s concentration in the bottom plane

time and velocity after 0.21 s of simulation when total number of RBCs is equal to $4.2 \cdot 10^6$. The results presented in Fig. 7 are generated according to the procedure called Lagrangian Particle Tracking. The selected results of DPM model of backfilling a morphologically complex surface by *RBC*s are also presented in Fig. 8 as distributions of velocity, shear stress and concentration of particles on the bottom of middle part of flow channel (exactly above cubes).

The effect of "pouring" particles is clearly captured in the developed DPM model of backfilling a morphologically complex surface by *RBC*s (Fig. 7). The flow of particles in a channel with cubes runs orderly, because the particle movement trajectories are enforced by the system of cubes. The simulation was carried out until the number of *RBC*s in the model increased, which in the simulation means leaving the *RBC*s out of the inlet part of flow channel, going through the middle part of flow channel and reaching the outlet part of flow channel. The distributions of velocity and shear stress (Fig. 8) indicate that arrangement of cubes on the lower surface of the channel organizes the flow of blood particles.

The analysis of the parameters influencing the backfilling process in the developed DPM model shows that the change in the shape of the bottom surface of the flow channel has a very large impact on these parameters, disproportionately greater than the change of the boundary condition.

5. Conclusions

The introduction of roughness as a boundary condition in the FVM model of flow channel led to a small reduction in relatively high values of shear stresses and led to a slower flow, even in the case of small surface roughness of the bottom plane of flow channel (several dozen of micrometers). However, the influence of cubes on the bottom layer in the FVM model on flow parameters is not very significant.

The influence of roughness as a boundary condition while computing mixture model of blood is less visible, only introduction of cubes increased significantly the computed values of blood velocities and shear stress. However, the mixture model leads to the lowest values of shear stress of all the applied models.

The introduction of the same roughness (several dozen of micrometers) as a boundary condition in the DPM model also led to a reduction in shear stresses and slowing down the flow, which additionally resulted in an increase of concentration of the *RBC*s on the bottom plane of flow channel, especially for the DPM model with cubes.

The arrangement of cubes more than one hundred micrometers high on the bottom plane of the flow channel organizes the flow of *RBC*s. The cubes strongly influence the shear stress, velocity and concentration of particles. The values of shear stress and velocity are significantly decreased, whereas the values of particle concentration significantly increase in comparison with DPM models with roughness.

Based on the simulation results, it is not possible to clearly determine which model most fully reflects the real conditions for the mechanism of pseudointima layer formation. However the most advanced model – DPM model with cubes is characterized by stress values of several Pascals, suggesting the correctness of the analysis. The next stage of the research is to conduct laboratory validation tests with the use of full human blood to verify the results obtained in this study.

Acknowledgements

The research was partially financed by the Polish National Science Centre under Project PRELUDIUM 16 2018/31/N/ST8/01085. Part of the work was executed under fundamental research no. 16.16.110.663 financed by AGH University of Science and Technology.

References

[1] ADAMCZUK K., WOLAŃSKI W., KASPERA W., *Analiza przepływu krwi w tętnicach mózgowych*, Aktualne Problemy Biomechaniki, 2016, 11, 9–14.

[2] ALIMOHAMADI H., SMITH A., NOWAK R., FOWLER V., RANGAMANI P., *Non-uniform distribution of myosin-mediated forces governs red blood cell membrane curvature through tension modulation*, PLOS Comput. Biol., 2020, 16, 1–26.

[3] BERIS A.N., HORNER J.S., JARIWALA S., ARMSTRONG M.J., WAGNER N.J., *Recent advances in blood rheology: A review*, Soft Condensed Matter, 2021, 1–22.

[4] BLAKE A.S.T., PETLEY G.W., DEAKIN C.D., *Effects of changes in packed cell volume on the specific heat capacity of blood: implications for studies measuring heat exchange in extracorporeal circuits*, Brit. J. Anaesth., 2000, 84, 28–32.

[5] BOWEN R.M., *Incompressible porous media models by use of the theory of mixtures*, Int. J. Eng. Sci., 1980, 18, 1129–1148.

[6] BURADI A., MAHALINGAM A., *Effect of stenosis severity on wall shear stress based hemodynamic descriptors using multiphase mixture theory*, J. Appl. Fluid Mech., 2018, 11, 1497–1509.

[7] CAI S., LI H., ZHENG F., KONG F., DAO M., KARNIADAKIS G.E., SURESH S., *Artificial intelligence velocimetry and microaneurysm-on-a-chip for three-dimensional analysis of blood flow in physiology and disease*, PNAS, 2021, 118, e2100697118.

[8] CAI Q., LIAO W., XUE F., WANG X., ZHOU W., LI Y., ZENG W., *Selection of different endothelialization modes and different seed cells for tissue-engineered vascular graft*, Bioact. Mater, 2021, 6, 2557–2568.

[9] CAPACCIO A., CASERTA S., GUIDO S., RUSCIANO G., SASSO A., *Dissolution of a surfactant-water lamellar phase investigated by combining time-lapse polarized light microscopy and confocal Raman spectroscopy*, J. Colloid. Interf. Sci., 2020, 561, 136–146.

[10] CEBECI T., BRADSHAW P., *Momentum transfer in boundary layers*, Hemisphere Publishing Corp., New York, 1977.

[11] DIEZ-SILVA M., DAO M., HAN J., LIM C.-T., SURESH S., *Shape and biomechanical characteristics of human red blood cells in health and disease*, MRS Bull, 2010, 35, 382–388.

[12] EL-ARAGI G.M., *Effect of electrohydraulic discharge on viscosity of human blood*, Phys. Res. Int., 2013, ID 203708.

[13] ERDEMIR A., GUESS T.M., HALLORAN J., TADEPALLI S.C., MORRISON T.M., *Considerations for reporting finite element analysis studies in biomechanics*, J. Biomech., 2012, 45, 625–633.

[14] FENG R., XENOS M., GIRDHAR M., KANG W., DAVENPORT J.W., DENG Y., BLUESTEIN D., *Viscous flow simulation in a stenosis model using discrete particle dynamics: a comparison between DPD and CFD*, Biomech. Model Mechanobiol., 2012, 11, 119–129.

[15] FLORMANN D.A.D., *Physical characterization of red blood cell aggregation*, Biological Physics, Universität des Saarlandes, 2017.

[16] FRASER K.H., ZHANG T., TASKIN M.E., GRIFFITH B.P., WU Z.J., *A quantitative comparison of mechanical blood damage parameters in rotary ventricular assist devices: shear stress, exposure time and hemolysis index*, J. Biomech. Eng., 2012, 134, 0810021.

[17] HAYASE T., SHIRAI A., SUGIYAMA H., HAMAYA T., *Measurement of frictional characteristics of red blood cells moving on a plate in plasma due to inclined centrifugal force*, Nippon Kikai Gakkai Ronbunshu, B Hen/Transactions of the Japan Society of Mechanical Engineers, Part B, 2002, 68, 3386–3391.

[18] HIMBERT S., ALSOP R.J., ROSE M., HERTZ L., DHALIWAL A., MORAN-MIRABAL J.M., VERSCHOOR C.P., BOWDISH D.M.E., KAESTNER L., WAGNER C., RHEINSTÄDTER M.C., *The Molecular Structure of Human Red Blood Cell Membranes from Highly Oriented*, Solid Supported Multi-Lamellar Membranes, Sci. Rep., 2017, 7, 39661.

[19] HORNER J.S., ARMSTRONG M.J., WAGNER N.J., BERIS A.N., *Investigation of blood rheology under steady and unidirectional large amplitude oscillatory shear*, J. Rheol., 2018, 62, 577–591.

[20] HUSSMANN B., PFITZNER M., ESCH T., FRANK T., *A stochastic particle-particle collision model for dense gas-particle flows implemented in the Lagrangian solver of ANSYS CFX and its validation*, 6th International Conference on Multiphase Flow, ICMF 2007, Leipzig, Germany, July 9–13, 2007, 1–16.

[21] JAMES M.E., PAPAVASSILIOU D.V., O'REAR E.A., *Use of computational fluid dynamics to analyze blood flow, hemolysis and sublethal damage to red blood cells in a bileaflet artificial heart valve*, Fluids, 2019, 4, 1–19.

[22] JARIWALA S., HORNER J.S., WAGNER N.J., BERIS A.N., *Application of population balance-based thixotropic model to human blood*, J. Non-Newton Fluid, 2020, 281, 104294.

[23] JØRGENSEN L.H., MØLLER V.S., REVSHOLM J., *Plasma viscosity: Evaluation of a new measuring method using microfluidic chip technology (microViscTM) for clinical use and determination of a new reference range*, Ann. Clin. Biochem., 2020, 57, 249–252.

[24] JUNG J., LYCZKOWSKI R.W., PANCHAL CH.B., HASSANEIN A., *Multiphase hemodynamic simulation of pulsatile flow in a coronary artery*, J. Biomech., 2006, 39, 2064–2073.

[25] KARAKI W., RAHUL, LOPEZ C.A., BORCA-TASCIUC D.A., DE S., *A continuum thermomechanical model of in vivo electrosurgical heating of hydrated soft biological tissues*, Int. J. Heat Mass Tran., 2018, 127, 961–974.

[26] KHANJANPOUR M.H., JAVADI A.A., *Experimental and CFD analysis of impact of surface roughness on hydrodynamic performance of a darrieus hydro (DH) turbine*, Energies, 2020, 13, 928.

[27] KIM J., ANTAKI J.F., MASSOUDI M., *Computational study of blood flow in microchannels*, J. Comput. Appl. Math., 2016, 292, 174–187.

[28] KOPERNIK M., TOKARCZYK P., *Development of multi-phase models of blood flow for medium-sized vessels with stenosis*, Acta Bioeng. Biomech., 2019, 21, 63–70.

[29] KURTYKA P., WALKE W., KACZMAREK M., *Fluid flow analysis using finite element method, determining the effects of the implantable mechanical heart valves on aortic blood flow*, Adv. Intell. Syst., 2016, 472, 255–266.

[30] LAIN S., ERNST M., SOMMERFELD M., *Study of colliding particle-pair velocity correlation in homogeneous isotropic turbulence*, Appl. Sci., 2020, 10, 9095.

[31] LEE B.-K., XUE S., NAM J., LIM H., SHIN S., *Determination of the blood viscosity and yield stress with a pressure-scanning capillary hemorheometer using constitutive models*, Korea – Aust. Rheol. J., 2011, 23, 1–6.

[32] LEE J., KIM I.G., OH Y.M., PARK C.-H., KIM C.S., *Preliminary study for measurement of shear stress and hemocompatibility using commercialized lab on a chip*, J. Nanoscie. Nanotechno., 2018, 18, 1123–1126.

[33] LIMA R., ISHIKAWA T., IMAI Y., YAMAGUCHI T., *Blood flow behavior in microchannels: past, current and future trends, Single and two-phase flows on chemical and biomedical engineering*, Dias R., Martins A.A., Lima R., Mata T.M. (Eds.), Bentham Science, 2012, 513–547.

[34] LIU H., LAN L., ABRIGO J., IP H.L., SOO Y., ZHENG D., WONG K.S., WANG D., SHI L., LEUNG T.W., LENG X., *Comparison of newtonian and non-newtonian fluid models in blood flow simulation in patients with intracranial arterial stenosis*, Front. Physiol., 2021, https://doi.org/10.3389/fphys.2021.718540

[35] LOVE A.I.J., GIDDINGS D., POWER H., *Gas-particle flow modeling: beyond the dilute limit*, Procedia Engineer., 2015, 102, 1426–1435.

[36] MAHDAVIMANESH M., NOGHREHABADI A.R., BEHBAHANINEJAD M., AHMADI G., DEHGHANIAN M., *Lagrangian particle tracking: model development*, Life Sci. J., 2013, 10, 34–41.

[37] MITCHELL D., HONNERY D., SORIA J., *Particle relaxation and its influence on the particle image velocimetry cross-correlation function*, Exp. Fluids, 2011, 51, 933.

[38] MENCONI M.J., POCKWINSE S., OWEN T.A., DASSE K.A., STEIN G.S., LIAN J.B., *Properties of blood-contacting surfaces of clinically implanted cardiac assist devices: gene expression, matrix composition, and ultrastructural characterization of cellular linings*, J. Cell. Biochem., 1995, 57, 557–573.

[39] MENTER F., *Two-equation eddy-viscosity turbulence models for engineering applications*, AIAA J, 2002, 40, 254–266.

[40] MORSI S.A., ALEXANDER A.J., *An investigation of particle trajectories in two-phase flow systems*, J. Fluid Mech., 1972, 55, 193–208.

[41] MURALI C., NITHIARASU P., *Red blood cell (RBC) aggregation and its influence on non-Newtonian nature of blood in microvasculature*, J. Model Mech. Mat., 2017, 1, 20160157.

[42] NANDA S.P., BASU MALLIK B., *A non-newtonian two-phase fluid model for blood flow through arteries under stenotic condition*, Int. J. Pharm. Bio. Sci., 2012, 2, 237–247.

[43] PATTANAPOL W., WAKES S.J., HILTON M.J., DICKINSON K.J., *Modeling of surface roughness for flow over a complex vegetated surface*, Int. J. Math. Phys. Eng. Sci., 2008, 2, 18–26.

[44] PICART C., PIAU J.-M., GALLIARD H., CARPENTIER P., *Human blood shear yield stress and its hematocrit dependence*, J. Rheol., 1998, 42, 1–12.

[45] PONDER E., *The specific heat and the heat of compression of human red cells, sickled red cells, and paracrystalline rat red cells*, J. Gen. Physiol., 1955, 38, 575–580.

[46] PRASHANTHA B., ANISH S., *Discrete-phase modelling of an asymmetric stenosis artery under different Womersley numbers*, Ara. J. Sci. Eng., 2019, 44, 1001–1015.

[47] RAFFI S., OZ M.C., SELDOMRIDGE J.A., FERRIS B., ASCH A.S., NACHMEN R.L., SHAPIRO F., ROSE E.A., LEVIN H.R., *Characterisation of hematopoetic cells arising on the textured surface on left ventriculat assist devices*, Ann. Thorac. Surg., 1995, 60, 1627–1632.

[48] ROSENTRATER K.A., FLORES R.A., *Physical and rheological properties of slaughterhouse swine blood and blood components*, T ASAE, 1997, 40, 683–689.

[49] SOUSA P.C., PINHO F.T., ALVES M.A., OLIVEIRA M.S.N., *A review of hemorheology: Measuring techniques and recent advances*, Korea – Aust. Rheol. J., 2016, 28, 1–22.

[50] SOMMERFELD M., HUBER N., *Experimental analysis and modelling of particle-wall collisions*, Int. J. Multiphas. Flow, 1999, 25, 1457–1489.

[51] THYAGARAJAN B., KUMAR M.P., SIKACHI R.R., AGRAWAL A., *Endocarditis in left ventricular assist device*, Intractable Rare Dis. Res., 2016, 5, 177–184.

[52] VAIDYA N., BARAGONA M., LAVEZZO V., MAESSEN R., VEROY K., *Simulation study of the cooling effect of blood vessels and blood coagulation in hepatic radiofrequency ablation*, Int. J. Hyperther., 2021, 38, 95–104.

[53] YU Z., TAN J., WANG S., *Enhanced discrete phase model for multiphase flow simulation of blood flow with high shear stress*, Sci. Prog., 2021, 104, 1–21.

[54] ZAHARI N.M., ZAWAWI M.H., SIDEK L.M., MOHAMAD D., ITAM Z., RAMLI M.Z., SYAMSIR A., ABAS A., RASHID M., *Introduction of discrete phase model (DPM) in fluid flow: a review*, AIP Conf. Proc., 2030, 2018, 020234-1-6.

[55] ZILLA P., DEUTSCH M., BEZUIDENHOUT D., DAVIES N.H., PENNEL T., *Progressive Reinvention or Destination Lost? Half a Century of Cardiovascular Tissue Engineering*, Front Cardiovasc. Med., 2020, 7, 1–159.